Molecular Basis for Microbial Adhesion to Geochemical Surfaces: Computer Simulation of *Pseudomonas aeruginosa* Adhesion to Goethite

Robert M. Shroll and T. P. Straatsma
Computational Biosciences, Biological Sciences Division, Pacific Northwest National Laboratory, Richland, Washington 99352 USA

ABSTRACT The adhesion of *Pseudomonas aeruginosa* to the goethite mineral is investigated using classical molecular simulation. A fragment model for goethite has been integrated into a fully atomistic membrane model. Properties for the resulting system are evaluated for a 1.5-ns simulation in the isothermal-isobaric ensemble. The response of the membrane to the presence of the mineral is investigated. Radial distribution functions are used to present an average picture of the hydrogen bonding. Orientational vectors, assigned to the saccharide groups, reveal the extent of the mineral's perturbations on the membrane. Significant structural changes were observed for the outermost saccharide groups, several of which rotate to form hydrogen bonds with the mineral surface. The structure of the inner core, and the corresponding integrity of the membrane, is maintained. The mineral surface dehydrates slightly in the presence of the membrane as saccharide hydroxyl groups compete with water molecules for hydrogen-bonding sites on its surface.

INTRODUCTION

Inorganic and organic pollutants are an ever-increasing byproduct of our industrialized world. Acid mine drainage, industrial and household wastewaters, and landfill leachate all contribute to metal and organic contamination of our soil and ground water (Ledin and Pedersen, 1996; Eccles, 1995; Islam et al., 2001). Similarly, a wide variety of petroleum and petroleum products are also being introduced as contaminants into the environment. Inadvertent releases occur during production, transportation, and storage of petroleum as well as seepage from natural deposits, leakage of gasoline from underground storage tanks, and marine spills such as from the Exxon Valdez (Balba et al., 1998; Bragg et al., 1994; Yuste et al., 2000). As a result of the Gulf War, millions of gallons of crude oil were released into the environment (Balba et al., 1998; Salam, 1996). One of the primary ways in which crude oil is eliminated from contaminated sites is through biodegradation by natural populations of microorganisms (Yuste et al., 2000). Bioremediation is emerging as a promising technology for treatment of these diverse systems of contaminated soil and ground water.

Mine wastes have been generated over the last several centuries of mining, the two primary mining wastes being mine tailings and waste rock. The drainage from these sources is typically acidic and contains high metal concentrations (Ledin and Pedersen, 1996). Conventional chemical methods of wastewater treatment involve introduction of an alkali to raise pH and precipitate the metals. However, this process is not selective, produces solid sludge for disposal, may have environmentally damaging effects of its own, and must be repeated to be effective. Determining the contribution of microbial processes to element cycling in mine wastes is necessary to avoid unexpected effects of the treatment on metal mobility and acid generation. This understanding is also important for the directed efforts of bioremediation techniques. Bacteria catalyze geochemical processes through their metabolism, and the understanding of mine waste environments requires inclusion of these processes.

Bacteria have important functions in bioremediation technology. Their cell walls contain binding sites for metal ions, which differ for the two basic cell wall types. Gram-positive bacterial binding sites are primarily carboxyl groups of the peptidoglycan. The primary binding sites for Gram-negative bacteria are carboxyl groups and phosphate groups in the lipopolysaccharide (LPS) units of the outer membrane (White et al., 1995; McLean and Beveridge, 1990; Lins and Straatsma, 2001). In anaerobic environments, some bacteria are able to substitute metal ions for molecular oxygen in the process of respiration. The ability to use Fe^{3+} and S^0 as terminal electron acceptors, while oxidizing organic contaminants to yield carbon dioxide, is shared by most of these dissimilatory metal-reducing bacteria (Lovley and Coates, 1997). Ion mobility is also indirectly affected through sulfide production and subsequent metal sulfide precipitation (Eccles, 1995; Ledin and Pedersen, 1996; White et al., 1995).

The adhesion of bacteria to mineral surfaces plays a central role in characterizing their contribution to the fate of contaminants in complex environmental systems by effecting microbial transport through soils, respiration redox chemistry, and ion mobility. Bacteria growing on a surface may reduce metal transport, whereas free-living bacteria that constitute mobile suspended particles may have a higher sorbing capacity and increase metal transport (Ledin and Pedersen, 1996). They may reduce mineral metal ions through direct contact or by reducing complexed ions. Here we investigate the adhesion of *Pseudomonas aeruginosa* to the mineral goethite using classical molecular simulation.

Submitted July 15, 2002, and accepted for publication October 23, 2002.

Address reprint requests to T. P. Straatsma, P.O. Box 999, MS K1-92, Richland, WA 99352; Tel.: 509-375-2802; E-mail: tps@pnl.gov.

Robert M. Shroll's present address is Spectral Sciences, 99 S. Bedford St., Suite 7, Burlington, MA 01803.

0006-3495/03/03/1765/08 $2.00

These simulations provide molecular level insight into bacterial interactions with mineral surfaces.

P. aeruginosa is a Gram-negative bacterium, which is commonly found in natural sources such as water, soil, and plant surfaces (Langley and Beveridge, 1999). It was one of three bacteria identified in well water contaminated by uranium mill tailings, where the native bacteria were shown to enzymatically reduce U^{6+} to U^{4+} (Abdelouas et al., 1998). The metal binding of *P. aeruginosa* has been shown to be affected by the mode of cell growth (grown planktonically or as biofilms) (Langley and Beveridge, 1999). *P. aeruginosa* has been widely studied as a source of microbial surfactants (Bai et al., 1997; Providenti et al., 1997; Banat et al., 2000). The mobility of bacteria through soils also has possible implications to in situ production of biosurfactants, which has far reaching bioremediation applications and is directly dependent on membrane to mineral adhesion.

Bacterial reduction of Fe^{3+} oxide is important because Fe^{2+} is a widespread ground-water contaminant, and other contaminant metals may often not be present at concentrations sufficient to support continued cell growth (Roden and Urrutia, 1999). Sources of Fe^{3+} such as goethite help to sustain bacterial populations and serve as the electron sinks for bacterial oxidation of hydrocarbons. Roden and Zachara (1996) showed the importance of bacterial interactions with mineral surfaces for bacterial Fe^{3+} reduction in goethite even in the presence of Fe-chelating ligands. The findings for their experimental system are consistent with direct association of bacteria, with surface sites on the oxide being required to initiate solid-phase Fe^{3+} reduction. They demonstrated that the surface area and site concentration of the solid phase controlled the rate and extent of microbial Fe^{3+} reduction. Ferric oxides and oxyhydroxides are important contributors to adsorption processes in the soil subsurface for a large number of cations and anions, due in part to their frequent occurrence as minerals and amorphous coatings with high specific area (Schwertmann and Cornell, 1991). Goethite crystals possess a high affinity for heavy metal contaminants (Schwertmann and Cornell, 1991; Hayes et al., 1987; Rustad et al., 1996b), where the predominant crystal plane of goethite needles has been shown to be (110) along the *c* direction and (021) at the needles' end (Schwertmann and Cornell, 1991; Weidler et al., 1996).

Here we present a detailed structural analysis of the adhesion of *P. aeruginosa* to a goethite mineral using parameterized classical simulations. Previously developed models for the mineral and for the membrane have been combined to yield the mineral-membrane simulation system (Lins and Straatsma, 2001; Shroll and Straatsma, 2003). Analysis of a 1.5-ns molecular dynamics trajectory reveals perturbations on the membrane due to the presence of the mineral. The exterior saccharide groups rotate themselves to form hydrogen bonds to the mineral surface. Inner core saccharide groups, which are responsible for maintaining the membrane integrity, exhibit little orientational change as a result of the mineral's presence. Much of the interaction between the mineral and membrane is mediated by a layer of water molecules on the mineral surface.

COMPUTATIONAL METHODS

Mineral model

The goethite fragment model of Shroll and Straatsma (2003) was used to represent the mineral surface. A fragment model was chosen over a periodic slab model allowing the membrane freedom to change the *xy* plane surface dimensions and preventing solvent from becoming trapped in the pore formed between layers. The mineral fragment was parameterized in the AMBER force field (Cornell et al., 1995), which allows for easy introduction of the model into biological simulations. The intermolecular potential is described as the sum of van der Waals and electrostatic point charge interactions. The mineral electrostatics were modeled by a set of atom-centered point charges based on restrained electrostatic potential fits (Bayly et al., 1993) using NWChem (Harrison et al., 2001; Straatsma and McCammon, 2001) to two-dimensional periodic Hartree-Fock calculations using CRYSTAL98 (Dovesi et al., 1998; Saunders et al., 1992). The intramolecular potential was parameterized to simulate a rigid structure with surface hydroxyl groups that are free to rotate in an AMBER-style torsional potential. The 110 mineral surface was terminated based on the work of Rustad et al. (1996a,b). This provides an average picture of mineral surface termination, and dissociation reactions are not allowed. A detailed description of the mineral model has been previously presented (Shroll and Straatsma, 2003).

Membrane model

The molecular model of Lins and Straatsma (2001) was used for the rough LPS membrane, and its construction is summarized here. The model was generated based on experimentally available structural data for the LPS monomer displayed in Fig. 1 (Sadovskaya et al., 1998). The lipid matrix of the outer membrane was constructed from a 40-molecule phosphatidylethanolamine membrane assembled at the bottom of 16 LPS molecules. Because each LPS unit is charged (-13 *e*), 104 Ca^{2+} ions were added to neutralize the system. Partial charges for the LPS atoms were determined by restrained electrostatic potential (Bayly et al., 1993) fits to Hartree-Fock SCF calculations using NWChem (Harrison et al., 2001). These charges were used with the AMBER95 (Cornell et al., 1995) and GLYCAM_93 (Woods et al., 1995) force field parameters. A weak restraining potential was applied to keep phosphatidylethanolamine headgroups in plane, which acts as a surrogate for the peptidoglycan layer. Here we also include the modifications of Cheatham et al. (1999) and weaken the restraining by two orders of magnitude (Shroll and Straatsma, 2002).

Mineral-membrane simulations

The initial configuration for the mineral-membrane simulation was generated from the final structures of the previous membrane simulation and mineral simulation (Shroll and Straatsma, 2002, 2003). The two simulation cells were joined together. Water molecules were removed from the outer core region of the membrane and from the mineral surface. The mineral and membrane were forced next to each other in a molecular dynamics simulation using a distance-restraining potential. The membrane was not allowed to move during the construction of the simulation cell to minimize unwanted perturbations on its structure. The restraining potential was applied until the membrane and mineral were in contact. The system was resolvated, and equilibrated for 200 ps with fixed solute in the NVT ensemble and then equilibrated with a fixed membrane (i.e., the mineral and

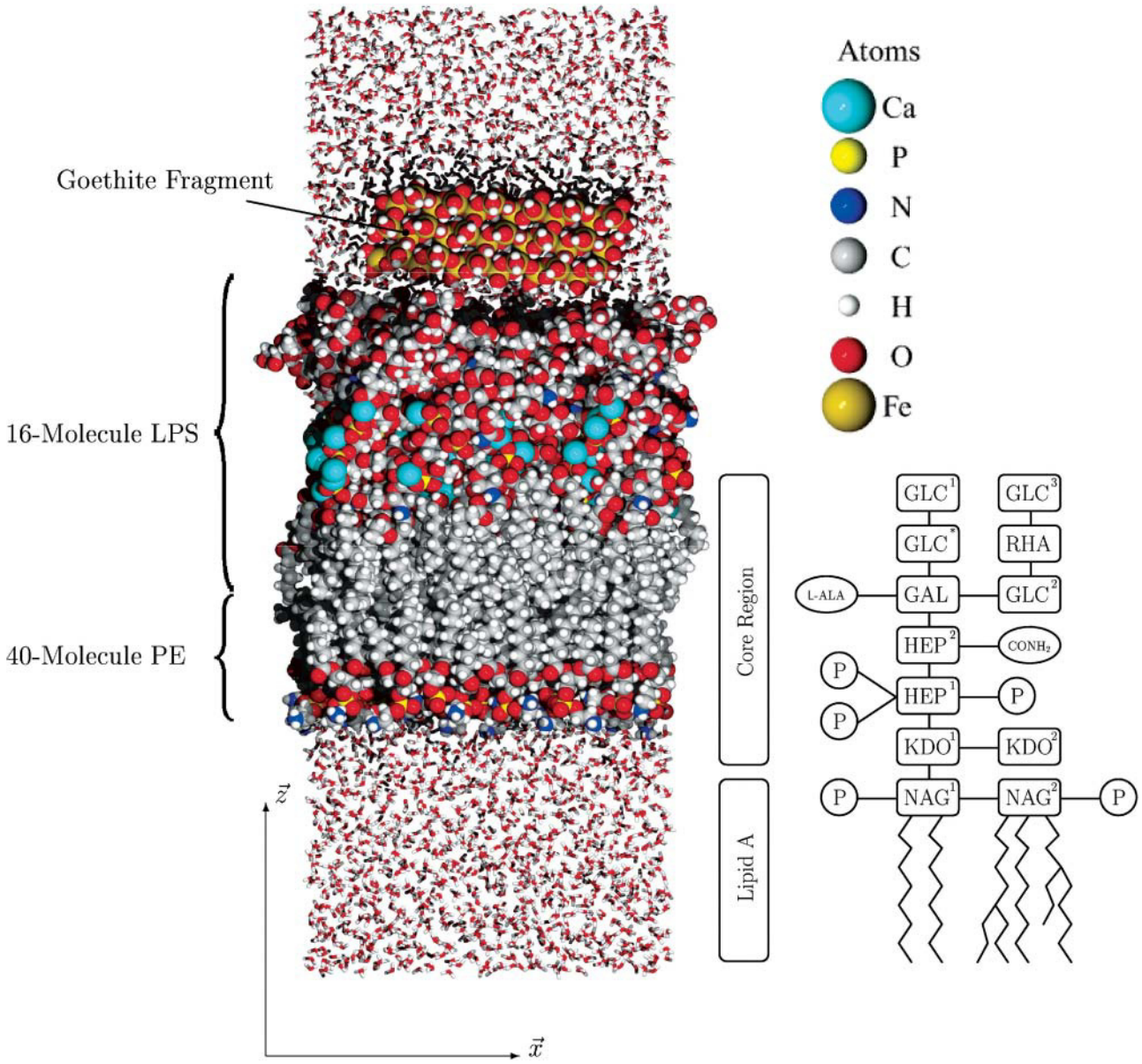

FIGURE 1 A space-filling representation of the mineral-membrane simulation cell. Two of the three simulation axes are displayed. The *y* axis is normal to the plane of the page with the positive direction facing out of the page. The coordinate origin is located at the geometric center of the membrane. Water molecules are displayed as sticks, and those with positive *y* values are not shown to reveal the mineral. The outer membrane is composed of 16 LPS units and 40 phosphatidylethanolamine units and a schematic of the LPS is provided. The LPS constituents are *N*-acetylglucosamine (NAG), 2-keto-3-deoxy-D-manno-octulosonic acid (KDO), phosphate (P), heptose (HEP), galactose (GAL), alanine (ALA), glucose (GLC), and rhamnose (RHA).

solvent were allowed to move) for 50 ps. This allowed the mineral to adjust its initial position, in the absence of the distance restraint, without perturbing the membrane structure. The resulting simulation cell dimensions were 36.14 Å × 48.57 Å × 154.80 Å ($x \times y \times z$), where the z axis is normal to the membrane surface. This initial configuration was equilibrated for 200 ps in the NPT ensemble before the start of data collection. A weak restraining potential was employed to keep the 110 mineral surface in the xy plane during the entire simulation insuring that the membrane interactions were with the 110 mineral surface and not with the fragment edges.

After equilibration, a 1.5-ns simulation of the mineral-membrane system was performed with periodic boundary conditions in the NPT ensemble using NWChem (Harrison et al., 2001). A target temperature of 300 K was maintained using a Berendsen thermostat with a temperature relaxation time of 0.1 ps (Berendsen et al., 1984). The target pressure of 1.025×10^5 Pa was maintained using a Berendsen pressure piston with relaxation time of 0.5 ps and a system compressibility of 4.53×10^{-10} m^2 N^{-1} with anisotropic coordinate scaling. The leapfrog integration method was used with a 2-fs time step (Hockney, 1970). A 1.0-nm cutoff was applied for direct interactions. The electrostatic interactions were evaluated for the periodically replicated system using the smooth particle mesh Ewald method with 64 grid points per dimension (Essmann et al., 1995). The extended simple point charge (SPC/E) water model was used (Berendsen et al., 1987). Each SPC/E water molecule consists of three atomic sites and has a rigid geometry with bond lengths of 1 Å and a tetrahedral bond angle.

Analysis

Radial and axial distribution functions are presented here to describe average structural features of the system. They are represented as either a function of the distance between atoms $g(r)$ or as a function of the z coordinate $g(z)$. To facilitate comparison of the distributions, both are expressed as ratios of a calculated number density to the number density of the SPC/E water model,

$$g = \frac{\rho_{\text{calc}}}{\rho_{\text{SPC/E}}}, \tag{1}$$

where the continuum of distances are calculated and assigned to discrete bins, which for $g(r)$ are spherical shells and for $g(z)$ hexahedrons.

The structural reorientation of the membrane was determined using vectors that define the orientation of the saccharide as follows. The vectors point from the center of geometry of the atoms OR, C1, and C2 to the center of geometry of the atoms C3, C4, and C5, using the common numbering of pyranose rings. This definition is identical to the one used in the analysis of the average motion of saccharide groups in the membrane (Shroll and Straatsma, 2002). The angle between this orientation vector and the z axis is θ, where $0° \le \theta \le 180°$. The vector z projection points away from the surface for $\theta = 180°$ and toward the surface for $\theta = 0°$. The angle between the xy projection and the y axis is ϕ, with $0° \le \phi < 360°$. The xy projection points in the negative y direction for $\phi = 0°$, in the x direction for $\phi = 90°$, in the y direction for $\phi = 180°$, and in the negative x direction for $\phi = 270°$. The probability that the vector has a given orientation of θ and ϕ is given by

$$P(\theta, \phi) = P(\theta)P(\phi) \tag{2}$$

$$P(>) = \frac{\langle h(>)\rangle}{\langle n\rangle N(>)}, \tag{3}$$

where $P(\theta)$ and $P(\phi)$ are the probabilities that the vector has an orientation with the specified angles, $>$ denotes either θ or ϕ, $\langle h(>)\rangle$ is the average number of vectors of a given orientation, $\langle n\rangle$ is the average total number of vectors sampled, and $N(>)$ is the angular-dependent normalization. For θ, the normalization is necessary because the vector sampling volume is a ring whose diameter is a function of the angle and for ϕ the normalization is independent of angle.

RESULTS AND DISCUSSION

A representative simulation cell is shown in Fig. 1. The mineral and membrane are rendered in a space-filling model, whereas the solvent is rendered in a stick model. The solvent has been included to help visualize the size of the cell. Two of the simulation axes are indicated in the image. The y axis is normal to the plane of the page with the positive direction pointing outward. The origin is at the geometric center of the membrane. Solvent with positive y values has been excluded from the figure to reveal the mineral.

Axial distribution functions for membrane atoms and water molecules are displayed in Fig. 2. These functions are analogous to the function for the isolated mineral in Fig. 6 of Shroll and Straatsma (2003) and the functions for the isolated membrane in Fig. 3 of Shroll and Straatsma (2002). The dashed line is the axial distribution function for all membrane atoms and is shown for part of the LPS region of the membrane only. The dotted line is the water axial distribution function. A comparison with Fig. 3 of Shroll and Straatsma (2002) reveals little change in the water

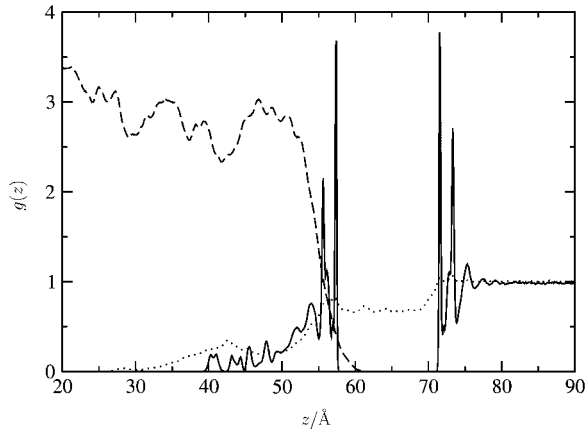

FIGURE 2 Axial distribution functions for all membrane atoms (*dashed*), water (*dotted*), and select water near the 110 mineral surface (*bold*). The origin of the plot is located in the phosphatidylethanolamine layer.

distribution function. Therefore the hydration of the membrane is not greatly affected by the presence of the mineral. The membrane atom distributions are very similar except for the outer 15 Å of the membrane. The presence of the mineral is evident from the depression in the water distribution (*dotted line*) in the region from $\sim z = 57$ Å to $z = 72$ Å. The distribution does not go to zero because the mineral is a fragment, allowing solvent to flow around the edges.

The solid line in Fig. 2 reveals the water axial distribution directly in front of both 110 mineral surfaces. The solution structure observed in the isolated mineral system (Shroll and Straatsma, 2003), is clearly seen. Both sides of the mineral possess this structure, even the side closest the membrane. The distribution of water near both 110 surfaces is compared in Fig. 3. In this figure, the water distribution extending toward the membrane is reflected through the center of the mineral (the xy plane with $z = 0$) to facilitate comparison

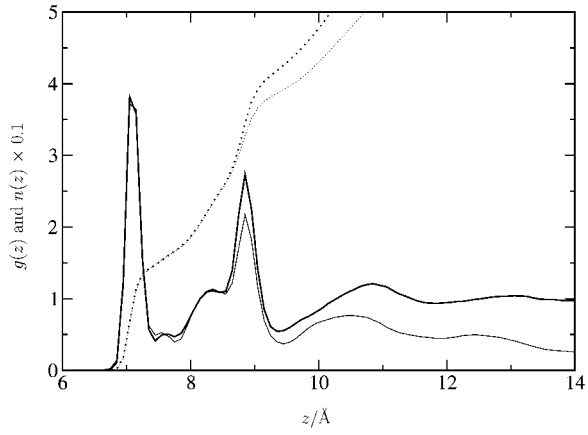

FIGURE 3 Axial distribution functions and the number of neighbors for water near the 110 mineral surfaces. Plots in bold are for the surface facing away from the membrane and plots in fine are for the surface facing toward the membrane. The neighbor function $n(z)$ has been scaled by 0.1 to show all four functions together.

between the distributions from both sides of the mineral. The average water density is equivalent out to 8.5 Å from the mineral center. A this point the water density for the surface near the membrane decreases, never reaching bulk behavior. The number of water molecules near the mineral surfaces is determined by integration of the distribution functions out to 9.5 Å. There are an average of 39 water molecules in the sampling region nearest to the membrane and 43 water molecules on the opposite side of the mineral. Therefore, four water molecules have been displaced in the region sampled by the axial distribution functions. There are 60 surface hydroxyl groups on each of the two 110 faces of the mineral. The number of reported water molecules associated with the mineral faces is significantly lower than the number of surface hydroxyl groups because the axial distribution sampling volume does not extend all the way to the edges of the mineral.

Analysis of hydrogen bonding between the mineral hydroxyl groups and the outermost saccharide groups of the membrane (GLC^3 and GLC^1) is presented in Fig. 4, *a* and *b*. In these figures, the distance between hydrogen atoms of the mineral and oxygen atoms of the saccharide groups are displayed in bold, whereas the distance between oxygen atoms of the mineral and hydrogen atoms of the saccharide groups is shown by the thin line. Solid lines are scaled radial distributions functions and dotted lines are the integrals representing the number of hydrogen bonds. Hydrogen bonding between mineral hydrogen atoms and membrane oxygen atoms is twice as likely than for the converse. Analysis of the trajectory revealed that hydrogen bonding occurs to the 110 mineral surface only and not to the edges. The average number of hydrogen bonds is 6.8, which is the sum of the four integral values at the first minimum in the corresponding radial distribution function. This is slightly greater than the calculated number of water molecules displaced near the mineral surface, because several hydrogen bonds were close enough to the mineral's edge to fall outside the volume sampled by the water distribution functions. These results indicate that in an aqueous environment, for the membrane to hydrogen bond to the mineral surface, it must displace hydrogen-bonded water molecules.

To determine the saccharide groups that hydrogen bond to the mineral surface and to quantify the extent of the perturbation on the membrane due to the mineral, saccharide orientation vectors were analyzed (see Analysis). The orientational distribution $P(\theta, \phi)$ for all 16 GLC^3 saccharide groups is given in Fig. 5 *a* for the isolated membrane and in Fig. 5 *b* for the mineral-membrane system. Results for the isolated membrane were calculated from previous membrane simulations (Shroll and Straatsma, 2002). Comparison of the two plots reveals a significant perturbation of the saccharide groups as a result of the presence of the mineral. Orientational vectors still favor being directed toward the inner core ($\theta = 0°$). The anisotropy with respect to vector precession about the z axis, however, has changed. Larger

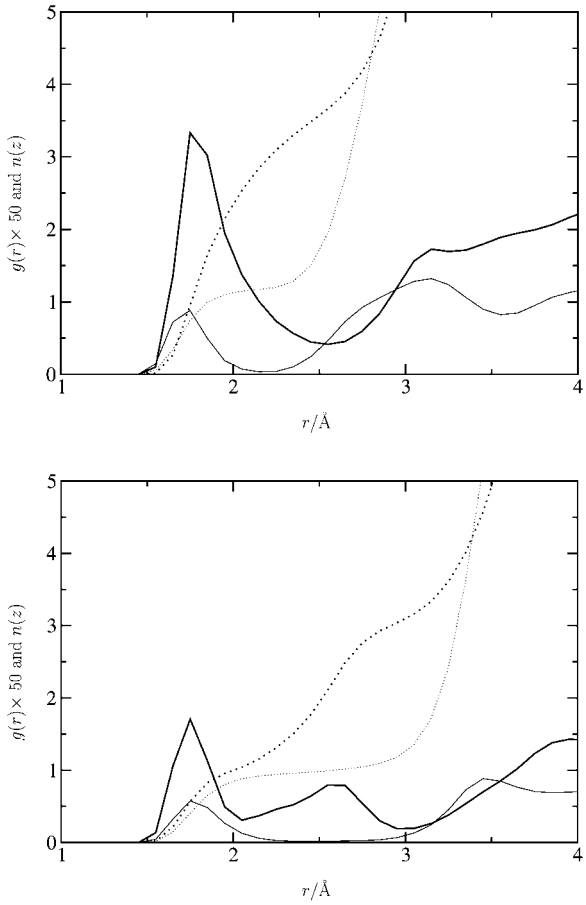

FIGURE 4 Hydrogen bonding between selected saccharide groups. Results for hydrogen bonding between mineral hydrogen atoms and membrane oxygen atoms are in bold, and the results for hydrogen bonding between mineral oxygen atoms and membrane hydrogen atoms are in fine. Solid lines are scaled radial distribution curves and dotted lines are the number of oxygen-hydrogen pairs. (*a*) Hydrogen bonding between GLC^3 and the mineral surface. (*b*) Hydrogen bonding between GLC^1 and the mineral surface.

peak heights for the mineral-membrane system indicate restrained motion of these saccharide groups relative to the isolated membrane. This is to be expected because of hydrogen bonding between the mineral and membrane.

Analysis of all 16 LPS units, in both the isolated membrane and the mineral-membrane systems, was performed and the LPS units with the largest changes in saccharide group orientation were determined. Orientation distribution plots for one of these LPS units are presented in Fig. 6, *a* and *b*. As was noted in our previous work, tall peaks with narrow bases indicate only a modest degree of saccharide motion, and a comparison of saccharide peaks from the inner core region to those of the outer core indicates greater motion in the outer core (Shroll and Straatsma, 2002). Because the motion of the saccharide groups is limited in the timescale of nanoseconds, comparison of Fig. 6 *a* with Fig. 6 *b* provides a good estimate of the perturbation of the mineral on the membrane.

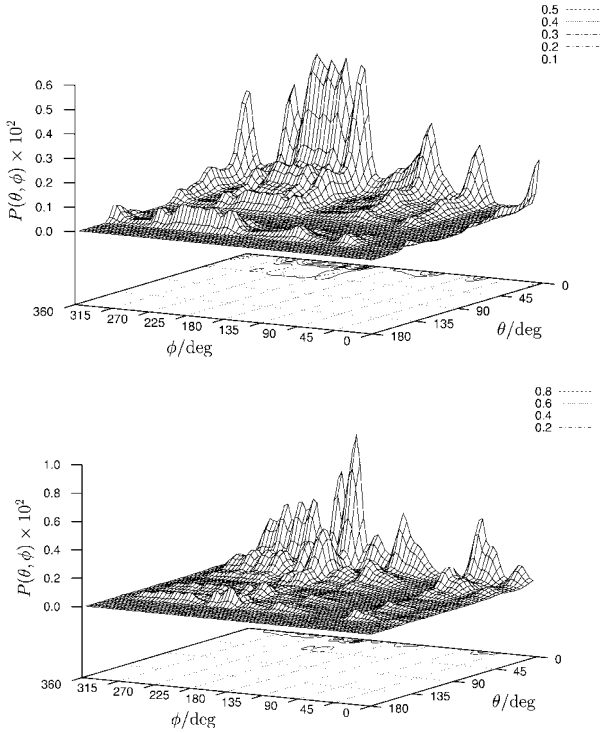

FIGURE 5 (*a*) The orientational probability $P(\theta, \phi)$ for all 16 GLC^3 saccharide groups for the isolated membrane system. (*b*) The orientational probability $P(\theta, \phi)$ for all 16 GLC^3 saccharide groups for the mineral-membrane system.

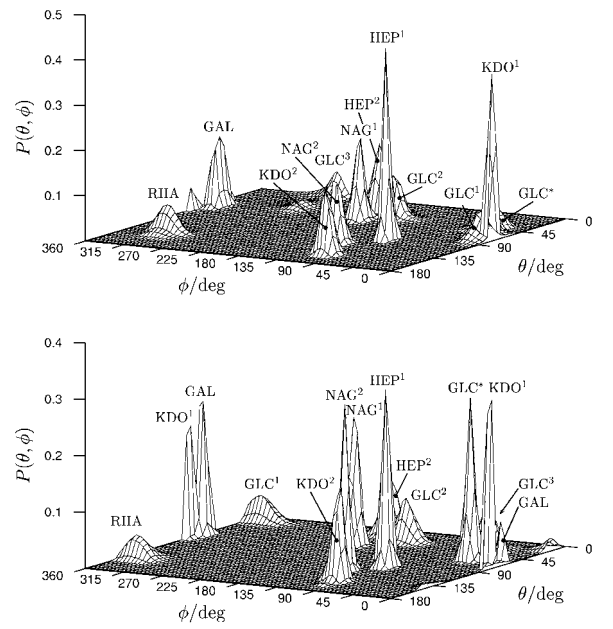

FIGURE 6 The orientational probability $P(\theta, \phi)$ for the same LPS unit of the membrane with and without the mineral present. The contribution to the total probability of each of the 12 saccharide groups has been normalized to 1 in both graphs. Saccharide abbreviations are defined in Fig. 1. (*a*) The orientational probability $P(\theta, \phi)$ for a single LPS of the isolated membrane. (*b*) The orientational probability $P(\theta, \phi)$ for a single LPS of the mineral-membrane simulation. The GLC^3 saccharide is hydrogen bonding to the 110 mineral surface and is the saccharide singled out in Fig 7.

The saccharide groups with only small changes in their average orientations are NAG^1, NAG^2, KDO^1, KDO^2, HEP^1, HEP^2, RHA, and GLC^2. They are located inside the membrane and do not come into direct contact with the mineral. There are significant changes in orientation of the GLC*, GLC^1, and GLC^3 saccharide groups, which are located near or at the surface of the membrane. Of these three, inspection of multiple snapshots shows that the GLC^3 saccharide of this LPS unit forms hydrogen bonds to the 110 mineral surface. The other saccharide groups of the LPS did not form hydrogen bonds with the surface and their orientational changes are smaller in magnitude. Snapshots of all 16 GLC^3 saccharide groups for both the isolated membrane and the mineral-membrane systems are shown in Fig. 7. The isolated membrane snapshot is located above the mineral-membrane snapshot. Arrows point to the saccharide from the same LPS unit analyzed in Fig. 6, *a* and *b*. Hydrogen bonds, represented by dashed lines, are shown between this saccharide and the mineral surface.

CONCLUSIONS

The inner core saccharide groups do not play a substantial role in the adhesion process over the timescale observed here. These groups are too far from the mineral surface to

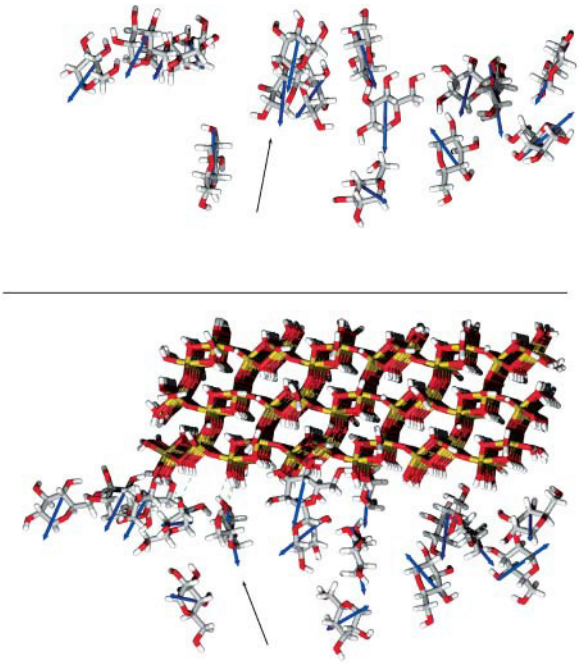

FIGURE 7 Snapshots for the GLC^3 saccharide groups. The top image is for the isolated membrane system and the bottom is for the mineral-membrane system. The black arrow indicates the saccharide forming a hydrogen bond to the mineral surface in Fig 6, *a* and *b*. The blue vectors are the orientational vectors used to analyze the motion of individual saccharide groups. Dashed lines identify hydrogen bonds, some of which are between equivalent hydrogen-bonding groups.

form hydrogen bonds and their average orientations were not significantly perturbed by its presence. The stability of the membrane hinges on the inner core region. Inasmuch as this region's response to the mineral was limited, the integrity of the membrane was maintained during the adhesion process.

The average hydration of the membrane was unaffected by the presence of the mineral except for a small region within 5 Å of the mineral surface. The goethite mineral surface only partially dehydrates to accommodate mineral-saccharide interactions. The results of these simulations indicate that the process of bacterial adhesion to mineral surfaces is dominated by the outermost membrane saccharide groups forming hydrogen bonds to the mineral surface. These saccharide groups must compete with water molecules to form hydrogen bonds with surface sites. The outer core saccharide groups are sufficiently mobile to respond to the mineral in a picosecond timescale by rotating into positions where they can form multiple hydrogen bonds without altering the structure of the inner core.

This work was supported in part by the Geosciences Research Program of the U.S. Department of Energy, Office of Basic Energy Sciences. Computing resources were available through a Computational Grand Challenge Application grant from the Molecular Science Computing Facility in the Environmental Molecular Sciences Laboratory, which is operated with funding from the Office of Biological and Environmental Research. The NWChem 4.0 computational chemistry package for massively parallel computers used in this study was developed by the Molecular Science Software group in the Theory, Modeling and Simulation Directorate of the Environmental Molecular Sciences Laboratory, Pacific Northwest National Laboratory, and supported by the Office of Biological and Environmental Research. Pacific Northwest National Laboratory is operated by Battelle Memorial Institute for the U.S. Department of Energy.

REFERENCES

Abdelouas, A., L. Yongming, W. Lutze, and H. E. Nuttall. 1998. Reduction of U(VI) to U(IV) by indigenous bacteria in contaminated ground water. *J. Contam. Hydrol.* 35:217–233.

Bai, G., M. L. Brusseau, and R. M. Miller. 1997. Biosurfactant-enhanced removal of residual hydrocarbon from soil. *J. Contam. Hydrol.* 25:157–170.

Balba, M. T., N. Al-Awadhi, and R. Al-Daher. 1998. Bioremediation of oil-contaminated soil: microbiological methods for feasibility assessment and field evaluation. *J. Microbiol. Methods.* 32:155–164.

Banat, I. M., R. S. Makkar, and S. S. Cameotra. 2000. Potential commercial applications of microbial surfactants. *Appl. Microbiol. Biotechnol.* 53:495–508.

Bayly, I. C., P. Cieplak, W. D. Cornell, and P. A. Kollman. 1993. A well-behaved electrostatic potential based method using charge restraints for deriving atomic charges: the RESP model. *J. Phys. Chem.* 97:10269–10280.

Berendsen, H. J. C., J. R. Grigera, and T. P. Straatsma. 1987. The missing term in effective pair potentials. *J. Phys. Chem.* 91:6269–6271.

Berendsen, H. J. C., J. P. M. Postma, W. F. van Gunsteren, A. DiNola, and J. R. Haak. 1984. Molecular-dynamics with coupling to an external bath. *J. Chem. Phys.* 81:3684–3690.

Bragg, J. R., R. C. Prince, E. J. Harder, and R. M. Atlas. 1994. Effectiveness of bioremediation for the Exxon Valdez oil spill. *Nature.* 368:413–418.

Cheatham 3rd, T. E., P. Cieplak, and P. A. Kollman. 1999. A modified version of the Cornell et al. force field with improved sugar pucker phases and helical repeat. *J. Biomol. Struct. Dyn.* 16:845–862.

Cornell, W. D., P. Cieplak, C. I. Bayly, I. R. Gould, K. M. Merz, D. M. Ferguson, D. C. Spellmeyer, T. Fox, J. W. Caldwell, and P. A. Kollman. 1995. A second generation force field for the simulation of proteins, nucleic acids and organic molecules. *J. Am. Chem. Soc.* 177:5179–5197.

Dovesi, R., V. R. Saunders, C. Roetti, M. Causá, N. M. Harrison, R. Orlando, and C. M. Zicovich-Wilson. 1998. CRYSTAL98 User's Manual. University of Turin, Turin, Italy.

Eccles, H. 1995. Removal of heavy-metals from effluent streams—why select a biological process? *Intern. Biodeter. Biodegrad.* 35:5–16.

Essmann, U., L. Perera, M. L. Berkowitz, T. Darden, H. Lee, and L. G. Pedersen. 1995. A smooth particle mesh Ewald method. *J. Chem. Phys.* 103:8577–8593.

Harrison, R. J., J. A. Nichols, T. P. Straatsma, M. Dupuis, E. J. Bylaska, G. I. Fann, T. L. Windus, E. Apra, J. Anchell, D. Bernholdt, P. Borowski, T. Clark, D. Clerc, H. Dachsel, B. de Jong, M. Deegan, K. Dyall, D. Elwood, H. Fruchtl, E. Glendenning, M. Gutowski, A. Hess, J. Jaffe, B. Johnson, J. Ju, R. Kendall, R. Kobayashi, R. Kutteh, Z. Lin, R. Littlefield, X. Long, B. Meng, J. Nieplocha, S. Niu, M. Rosing, G. Sandrone, M. Stave, H. Taylor, G. Thomas, J. van Lenthe, K. Wolinski, A. Wong, and Z. Zhang. 2001. NWChem, A Computational Chemistry Package for Parallel Computers, Version 4.0.1. Pacific Northwest National Laboratory, Richland, WA, USA.

Hayes, K. F., A. L. Roe, G. E. Brown, K. O. Hodgson, J. O. Leckie, and G. A. Parks. 1987. In situ x-ray absorption study of surface complexes: selenium oxyanions on α-FeOOH. *Science.* 238:783–786.

Hockney, R. W. 1970. The potential calculations and some applications. *Methods Comput. Phys.* 9:136–211.

Islam, J., N. Singhal, and M. O'Sullivan. 2001. Modeling biogeochemical processes in leachate-contaminated soils: a review. *Transport in Porous Media.* 43:407–440.

Langley, S., and T. J. Beveridge. 1999. Metal binding by *Pseudomonas aeruginosa* PAO1 is influenced by growth of cells as a biofilm. *Can. J. Microbiol.* 45:616–622.

Ledin, M., and K. Pedersen. 1996. The environmental impact of mine wastes—roles of microorganisms and their significance in treatment of mine wastes. *Earth-Sci. Rev.* 41:67–108.

Lins, R. D., and T. P. Straatsma. 2001. Computer simulation of the rough lipopolysaccharide membrane of *Pseudomonas aeruginosa. Biophys. J.* 81:1037–1046.

Lovley, D. R., and J. D. Coates. 1997. Bioremediation of metal contamination. *Curr. Opin. Biotechnol.* 8:285–289.

McLean, R. J. C., and T. J. Beveridge. 1990. Metal-binding capacity of bacterial surface and their ability to form mineralized aggregates. *In* Microbial Mineral Recovery. H. L. Ehrlich and C. L. Brierley, editors. McGraw-Hill, New York. 185–222.

Providenti, M. A., C. A. Flemming, H. Lee, and J. T. Trevors. 1997. Effect of addition of rhamnolipid biosurfactants or rhamnolipid-producing *Pseudomonas aeruginosa* on phenanthrene mineralization in soil slurries. *FEMS Microbiol. Ecol.* 17:15–26.

Roden, E. E., and M. M. Urrutia. 1999. Ferrous iron removal promotes microbial reduction of crystalline iron(II) oxides. *Environ. Sci. Technol.* 33:1847–1853.

Roden, E. E., and J. M. Zachara. 1996. Microbial reduction of iron(III) oxides: influence of oxide surface area on potential for cell growth. *Environ. Sci. Technol.* 30:1618–1628.

Rustad, J. R., A. R. Felmy, and B. P. Hay. 1996a. Molecular statics calculations for iron oxide and oxyhydroxide minerals: toward a flexible model of the reactive mineral-water interface. *Geochim. Cosmochim. Acta.* 60:1553–1562.

Rustad, J. R., A. R. Felmy, and B. P. Hay. 1996b. Molecular statics calculations of proton binding to goethite surfaces: A new approach to estimation of stability constants for multisite surface complexation models. *Geochim. Cosmochim. Acta.* 60:1563–1576.

Sadovskaya, I., J. R. Brisson, J. S. Lam, J. C. Richards, and E. Altman. 1998. Structure elucidation of the lipopolysaccharide core regions of the wild-type strain PAO1 and O-chain-deficient mutant strains AK1401 and AK1012 from *Pseudomonas aeruginosa* serotype O5. *Eur. J. Biochem.* 255:673–684.

Salam, A. A. 1996. Remediation and rehabilitation of oil-lake beds. *In* Environmental Disaster. N. Al-Awadhi, M. T. Balba, and C. Kamizawa, editors. Elsevier, Amsterdam. 117–139.

Saunders, V. R., C. Freyria-Fava, R. Dovesi, L. Salasco, and C. Roetti. 1992. On the electrostatic potential in crystalline systems where the charge density is expanded in Gaussian functions. *Mol. Phys.* 77:629–665.

Schwertmann, U., and R. M. Cornell. 1991. Iron Oxides in the Laboratory: Preparation and Characterization. Wiley-VCH, Weinheim, Germany.

Shroll, R. M., and T. P. Straatsma. 2003. A fragment model for the goethite mineral. *Molecular Simulations.* 29:1–11.

Shroll, R. M., and T. P. Straatsma. 2002. Molecular structure of the outer bacterial membrane of *Pseudomonas aeruginosa* via classical simulation. *Biopolymers.* 65:395–407.

Straatsma, T. P., and J. A. McCammon. 2001. Load balancing of molecular dynamics simulation with NWChem. *IBM Systems Journal.* 40:328–341.

Weidler, P. G., T. Schwinn, and H. E. Gaub. 1996. Vicinal faces on synthetic goethite observed by atomic force microscopy. *Clays Clay Miner.* 44:437–442.

White, C., S. C. Wilkinson, and G. M. Gadd. 1995. The role of microorganisms in biosorption of toxic metals and radionuclides. *International Biodeterioration & Biodegredation.* 35:17–40.

Woods, R. J., A. R. Dwek, and C. J. Edge. 1995. Molecular mechanical and molecular simulations of glycoproteins and oligosaccharides. 1. GLYCAM_93 parameter development. *J. Phys. Chem.* 99:3832–3846.

Yuste, L., M. E. Corbella, M. J. Turiégano, U. Karlson, A. Puyet, and F. Rojo. 2000. Characterization of bacterial strains able to grow on high molecular mass residues from crude oil processing. *FEMS Microbiol. Ecol.* 32:69–75.